Atmospheric Research 265 (2022) 105919

Contents lists available at ScienceDirect

Atmospheric Research

journal homepage: www.elsevier.com/locate/atmosres

Mimicking atmospheric photochemical modeling with a deep neural network

Jia Xing [a,b], Shuxin Zheng [c,**], Siwei Li [d,**], Lin Huang [c], Xiaochun Wang [a,b], James T. Kelly [e], Shuxiao Wang [a,b,*], Chang Liu [c], Carey Jang [e], Yun Zhu [f], Jia Zhang [c], Jiang Bian [c], Tie-Yan Liu [c], Jiming Hao [a,b]

[a] State Key Joint Laboratory of Environmental Simulation and Pollution Control, School of Environment, Tsinghua University, Beijing 100084, China
[b] State Environmental Protection Key Laboratory of Sources and Control of Air Pollution Complex, Beijing 100084, China
[c] Microsoft Research Asia, Beijing 100080, China
[d] School of Remote Sensing and Information Engineering, Wuhan University, Wuhan 430079, China
[e] Office of Air Quality Planning and Standards, U.S. Environmental Protection Agency, Research Triangle Park, NC 27711, USA
[f] College of Environment and Energy, South China University of Technology, Guangzhou Higher Education Mega Center, Guangzhou 510006, China

ARTICLE INFO

Keywords:
Atmospheric photochemistry
Ozone
Emissions
Meteorology
Chemical transport model
Deep learning

ABSTRACT

Fast and accurate prediction of ambient ozone (O_3) formed from atmospheric photochemical processes is crucial for designing effective O_3 pollution control strategies in the context of climate change. The chemical transport model (CTM) is the fundamental tool for O_3 prediction and policy design, however, existing CTM-based approaches are computationally expensive, and resource burdens limit their usage and effectiveness in air quality management. Here we proposed a novel method (noted as DeepCTM) that using deep learning to mimic CTM simulations to improve the computational efficiency of photochemical modeling. The well-trained DeepCTM successfully reproduces CTM-simulated O_3 concentration using input features of precursor emissions, meteorological factors, and initial conditions. The advantage of the DeepCTM is its high efficiency in identifying the dominant contributors to O_3 formation and quantifying the O_3 response to variations in emissions and meteorology. The emission-meteorology-concentration linkages implied by the DeepCTM are consistent with known mechanisms of atmospheric chemistry, indicating that the DeepCTM is also scientifically reasonable. The DeepCTM application in China suggests that O_3 concentrations are strongly influenced by the initialized O_3 concentration, as well as emission and meteorological factors during daytime when O_3 is formed photochemically. The variation of meteorological factors such as short-wave radiation can also significantly modulate the O_3 chemistry. The DeepCTM developed in this study exhibits great potential for efficiently representing the complex atmospheric system and can provide policymakers with urgently needed information for designing effective control strategies to mitigate O_3 pollution.

1. Introduction

The ambient ozone (O_3) exerts great damages in human health (Murray et al., 2020; Wang et al., 2020) and natural ecosystem (Grulke and Heath, 2020), leading to 365 thousand premature deaths worldwide in the year 2019. In China, O_3 has gained increased attention recently due to worsened O_3 pollution in recent years (Lu et al., 2020; Ding et al., 2019a). The ambient O_3 is mainly formed from two important precursors of nitrogen oxides (NO_x) and volatile organic compounds (VOC) through complex photochemical processes in which both anthropogenic emissions and meteorological factors are involved (Gipson et al., 1981; Hu et al., 2021). Many studies suggested that the unexpected O_3 increases in China might be due to both unbalanced precursor (i.e., NO_x and VOC) emission controls and meteorological conditions favorable for O_3 formation (Wang et al., 2019a, 2019b; Ding et al., 2019a; Ma et al., 2019; Yang et al., 2021). Therefore, the design of

* Corresponding author at: State Key Joint Laboratory of Environmental Simulation and Pollution Control, School of Environment, Tsinghua University, Beijing 100084, China.
** Corresponding authors.
E-mail addresses: Shuxin.Zheng@microsoft.com (S. Zheng), siwei.li@whu.edu.cn (S. Li), shxwang@tsinghua.edu.cn (S. Wang).

https://doi.org/10.1016/j.atmosres.2021.105919
Received 27 September 2021; Received in revised form 30 October 2021; Accepted 5 November 2021
Available online 9 November 2021

effective control strategies requires accurate and quick estimation of the O_3 response to variations in emissions and meteorology.

However, predicting the O_3 response to emissions and meteorology variations is challenging due to the high nonlinearity associated with atmospheric photochemical processes (Seinfeld and Pandis, 2012). The chemical transport model (CTM) is the fundamental tool for simulating the O_3 concentrations with the inputs of precursor emissions and meteorological factors across time and space. However, due to its large computational burdens associated with solving multiple differential equations (Brasseur and Jacob, 2017), most previous studies performed scenario analysis to investigate the influence of meteorology and emissions separately, either by reducing emissions under constant meteorological conditions or by modulating meteorology under constant emissions (Gilliland et al., 2008; Xing et al., 2011a). The nonlinear response of O_3 to emission changes has also been explored with advanced CTM-based tools (Dunker et al., 2002; Xing et al., 2011b; Wild et al., 2012; Kwok et al., 2015; Xing et al., 2017a; Turnock et al., 2018; Cohan et al., 2005), but these tools are generally resource intensive and limit the exploration of nonlinear O_3 responses to combined variations in emissions and meteorology. For instance, studies have revealed that future climate change may challenge efforts to continually improve air quality (Stowell et al., 2017; Hong et al., 2019). Yet the question of how meteorology influences the effectiveness of emission controls still has not been well addressed. A method to efficiently quantify the influence of meteorological variations on the response of O_3 to emission changes is therefore urgently needed.

The reduced-form models have been gained great attention for their high efficiency in predicting atmospheric composition and estimating health effects. For example, the Intervention model for air pollution (InMAP) was designed to be an alternative to CTMs for estimating air quality response by solving a steady-state solution to reaction-advection-diffusion equation (Tessum et al., 2017). The response surface model (RSM) was designed to create the nonlinear response of air pollution to precursor emissions through statistic regression based on multiple CTM simulations (Xing et al., 2011b). Such reduced-form models can be further implemented into integrated assessment model for optimizing the control strategy, and be also helpful for data assimilation and emission inventory inversion based on the nonlinear response of concentrations to emissions provided by the reduced-form models (Xing et al., 2020a, 2020b).

Deep learning technology, such as convolutional neural networks (CNNs) and recurrent neural networks (RNNs), has demonstrated skill in representing the highly nonlinear and interactive relationships in the atmospheric system (Cabaneros et al., 2019; Womack et al., 2019; Kelp et al., 2020). Our previous studies suggest that the air pollution response to emission changes can be inferred from the baseline concentrations of certain chemical indicators determined by the emissions and meteorology (Xing et al., 2020c). It is expected that pollutant concentrations are also predictable from emissions and meteorology using deep learning methods. More importantly, deep-learning representations of the geophysical relationships of CTMs can substantially enhance the efficiency of predicting the O_3 response by avoiding the complex numerical calculations in CTM, and thus enable examination of the O_3 response to emissions and meteorology in a much higher dimensional space than traditional CTM studies. Such methods would provide essential information to policymakers to understand air pollution formation mechanisms and design proper control policies to continually improve air quality. While, the major concern about the deep learning models is about its interpretability. Besides, the feature selection in deep learning models is also challenging for well reproducing the whole atmospheric system which has a great number of variables in the CTM simulation.

Overall, the key questions are how to design a suitable neural network and how well such a network can replicate the CTM in revealing the inner relationships between O_3 and emissions and meteorology. To address these questions, we propose a novel deep learning neural network structure (noted as DeepCTM) to reproduce the CTM-predicted O_3. The properties of the new DeepCTM are examined for its ability to capture the nonlinearity of the O_3 response to emissions and meteorology.

2. Methods

2.1. Dataset preparation

To establish the dataset for DeepCTM training, we used the Community Multiscale Air Quality (CMAQ) model, version 5.2, which is one of the most commonly used CTMs for simulating the air pollutant concentrations (Appel et al., 2018). Meteorological fields were developed from simulations with the Weather Research and Forecasting (WRF) model, version 3.8 (Skamarock et al., 2008). The CMAQ and WRF model configurations are the same as in our previous studies (Ding et al., 2019a, 2019b). The Carbon Bond 6 (Sarwar et al., 2008) and AERO6 (Appel et al., 2013) mechanisms were used to represent gas-phase and particulate matter chemistry, respectively. Anthropogenic emissions are based on the bottom-up ABaCAS-EI inventory developed by Tsinghua University with a high spatial and temporal resolution (Zheng et al., 2019; Xing et al., 2020d). Biogenic emissions were based on the Model for Emissions of Gases and Aerosols from Nature (MEGAN) (Guenther et al., 2012). The performance of WRF and CMAQ for simulating meteorological variables and air pollutant concentrations has been thoroughly evaluated against observations in our previous studies (Ding et al., 2019a, 2019b).

The study domain covers most of East Asia using 182 (row) $\times$ 232 (column) horizontal grid cells with 27 km $\times$ 27 km resolution. In addition to national averages, our analysis also focuses on three key regions in China that suffer the most serious O_3 pollution, including North China Plain, the greater Yangtze River Delta, and Southeast China (Fig. S1).

2.2. DeepCTM structure

Although deep learning models can act as a universal approximator to represent any nonlinear system (Csáji, 2001), it is quite challenging for them to approximate the complicated atmospheric system. The challenges are due in part to unsatisfactory performance in neural-based solvers for partial differential equations (Hsieh et al., 2019). To address these challenges, key inductive biases must be introduced (Goyal and Bengio, 2020) when designing the features and architecture of the deep learning model.

Since the DeepCTM aims to mimic the CMAQ simulation, the features are selected from the original inputs for CMAQ model. First, we limit the initial concentration fields to only two species including NO_2 and O_3. Since VOC has too many species, including them will significantly enlarge the computational demand and the error accumulation (i. e., the output from previous step will be used as the initial concentration for next step prediction). CO is not included for its relative long lifetime thus has little impacts at a short period of time. In addition, we carefully construct 10 feature maps that are sufficient to represent the response relationship between emissions and O_3 concentrations. The feature data consist of two emission variables including total VOC emissions and NO_x emissions; six meteorological variables including planetary boundary layer (PBL) height, wind speed (WS), short-wave radiation (SWR), convective velocity scale (WSTAR), 2-m temperature (T2) and humidity (Q2); transport fluxes including U- and V- direction winds (UV-wind) which represent the movement between neighboring grid cells following the horizontal wind direction; and a time-independent variable terrain height (normalized with mean 0 and variance 1) to represent the geographical information. The feature data will be fed into the DeepCTM to mimic the CMAQ simulation.

Second, we carefully design the structure of DeepCTM to capture the spatial and temporal relationships among local emissions, meteorology

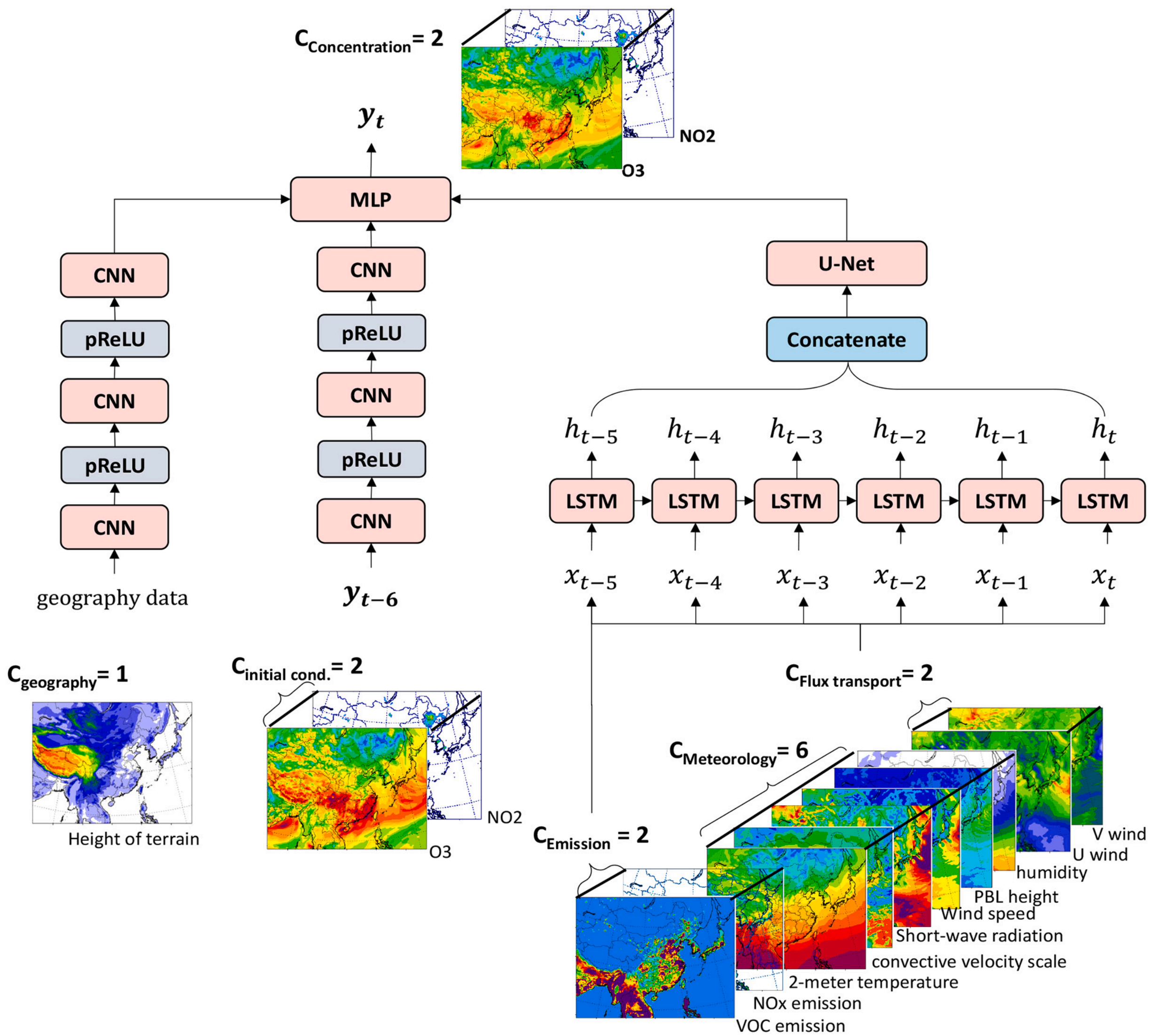

Fig. 1. The model architecture of the DeepCTM for predicting O_3 variations with emissions and meteorology. CNN: convolution network; LSTM: long short term memory; U-Net structure (2-layers): a u-shaped architecture with a down sample function (max pooling) and a deconvolution function (up convolution); MLP: multiple layers of perceptrons with threshold activation; pReLU: the parametric rectified linear unit is used as the activation function.

and the concentrations to be predicted. Specifically, similar to our previous study (Huang et al., 2021), we use stacked convolutional layers to maintain spatial information through the network and better extract the exclusive characteristics from the inputs, and one long short-term memory (LSTM) to aggregate information from time series data to mimic the accumulation of pollutants from historical processes. Additionally, we use a U-Net branch which is a widely adopted pixel-to-pixel model to effectively utilize neighbor information. To stabilize the optimization procedure, we employ two key components to smooth the energy landscape: (i) batch normalization of the activations (Santurkar et al., 2018) and (ii) skip connections to eliminate the problematic singularities in deep networks (Orhan and Pitkow, 2018). The detailed architecture is presented in Fig. 1. The 10 feature maps in past 6 h data are concatenated and fed into the LSTM with U-Net branch of a two-layer structure detailed in our previous study (Huang et al., 2021), and further combined with geography data and initial concentration at *t-6* (i.e., 6 h before, y_{t-6}) into the MLP (multiple layers of perceptrons with threshold activation) to predict the concentrations at *t* (i.e., y_t). Here we set 6 h instead of 1 h as the model time step for the consideration that O_3 could be substantially changed during the 6 h periods, resulting in large

Table 1
Summary of training and testing dataset.

Case	Dateset name	Anthopogenic emission	Meteorological conditions and biogenic emission	For training	For testing
1	e2017-base	2017	2017 baseline	√	
2	e2017-double	2017 doubled	2017 baseline	√	
3	e2050L-BCC_ssp126	2050 low	2050 ssp126 simulated with BCC model	√	
4	e2050H-BCC_ssp585	2050 high	2050 ssp585 simulated with BCC model		√
5	e2050L-ensmean_ssp126	2050 low	2050 ssp126 ensembled with 5 models		√
6	e2050L-ensmean_ssp585	2050 low	2050 ssp585 ensembled with 5 models		√
7	e2050H-ensmean_ssp126	2050 high	2050 ssp126 ensembled with 5 models		√
8	e2050H-ensmean_ssp585	2050 high	2050 ssp585 ensembled with 5 models		√

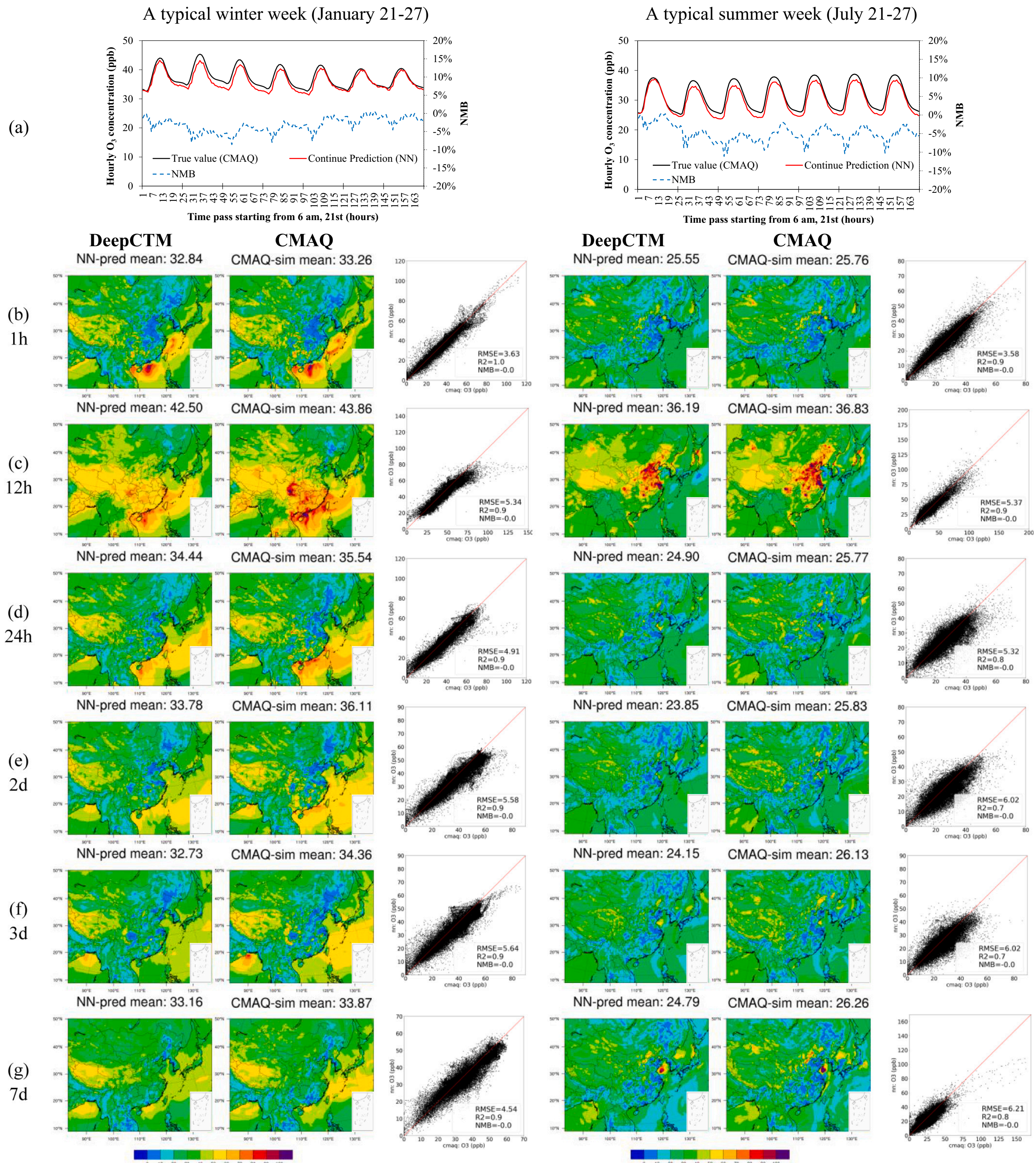

Fig. 2. DeepCTM performance in predicting O_3 variations with emissions and meteorology (test: Case #4).

discrepancy between the initial condition (one feature) and prediction (label) which is enough for the NN model to learn the influence of emissions and meteorological factors. More important, the number of accumulation steps for a whole day can be substantially reduced to well control the accumulation errors. The trained model can be deployed for either single step (no accumulation) or through multiple steps with the initialized conditions predicted from previous step. The single-step application can be helpful for identifying the driven factors for O_3 formation within 6-h period with high accuracy, while the multiple-step application can fully replicate the CMAQ simulation with moderate accuracy, since it can predict the O_3 concentration just using the inputs for CMAQ simulation with high efficiency (i.e., a few seconds with well-trained DeepCTM compared to hours of simulation with CMAQ).

2.3. Training and testing

We conducted WRF-CMAQ simulations for eight cases based on different combinations of emissions and meteorological conditions, as summarized in Table 1. In addition to the base-year simulation of 2017 (Case 1), we conducted simulations with doubled 2017 emissions (Case 2), as well as with various future emissions and meteorological conditions downscaled from the simulation of global climate models (Case 3–8) to explore the domain transfer capabilities of DeepCTM (Liu et al., 2021).

We selected two future pathways of a shared socioeconomic pathway 126 (ssp126) and a reference fossil fuel scenario (ssp585) to represent low- and high-level global warming conditions in 2050, as detailed in Liu et al. (2021). The anthropogenic emissions in 2050 at both low and high levels are used to represent the variation of emissions. The comparison of the distribution of feature data in base and future years (Case 1, 3–4) is given in Fig. S2-S3. In general, most features exhibit similar spatial and temporal distributions, while the emissions in the 2050-low case are much smaller (by 60–80%) than in the 2050-high and 2017 cases, and the 2-m temperatures in 2050s are higher (by 1-2 K) than in 2017 (Liu et al., 2021).

The hourly data of the first 7 days in each month of Case 1–3 (i.e., total 6048 records) are used for training, to better represent the variation of emissions from high to low levels and change of meteorology from current to future warming conditions. The remaining days of Case 1–3 as well as all days in Case 4–8 are used for testing. We did not select additional datasets for training due to the limited GPU memory (the task was accomplished on a NVIDIA DGX station with maximum capacity of 128 GB).

We randomly cropped the feature maps by the size of 60 for data augmentation to improve the performance of the CNN in dealing with the low-level task. That is because the atmospheric process mainly happens within certain distance in an hour, implying that the neighbor grid cells are more important rather than the one far away from the target (low-level task). In addition, using random cropping can enhance the variation of the training samples, also significantly reduced the memory requirement during the training by avoiding using high-resolution maps.

The Mean Squared Error loss was used for training, with 5000 epochs which is sufficient to achieve good performance in both training and testing. The learning rate starts from 0.001 and linearly decay to zero at the end of training. The loss variation of the training process is given in Fig. S4. One thing should be noted that since the training loss is computed over the cropped maps but the test loss is computed over the entire map, therefore the trend of loss curves is more meaningful than the quantitative comparison between training and test loss.

We have trained our model with both normalized and unnormalized data, and the performance gap is marginal. Considering the importance of feature on prediction is examined by through a certain amount of perturbation, we didn't normalize the feature data except for terrain height.

We calculated model performance statistics using the normalized mean bias (NMB), the root mean square error (RMSE), and R-squared (R^2). Model performance is also thoroughly examined through its ability to characterize the nonlinear response of O_3 to emission and meteorological factors.

3. Results

3.1. Performance evaluation for predicting the temporal and spatial O_3 patterns

After 5000 epochs, the trained DeepCTM can well reproduce the CTM-simulated hourly O_3 variation across the whole year. The RMSEs and NMBs for the training dataset are 3–4 ppb and ± 1% respectively, and R^2 values are very close to 1 (see Fig. S5). The RMSEs for the testing dataset (4–5 ppb) are slightly worse than for the training dataset but the NMBs are still within ±1%. Such good performance in both the training and testing dataset suggest that the DeepCTM has good generalization capabilities.

We further applied the trained DeepCTM to Case 4 with completely different emissions and meteorological conditions from the training dataset (Case 1–3). As presented in Fig. 2, the results suggest that the DeepCTM can well reproduce the spatial distribution of CTM-simulated O_3, as demonstrated by the comparison of two representative days from the testing dataset (i.e., the 21st day in January and July, which represent winter and summer, respectively in Case 4). The DeepCTM predictions for O_3 at the next 6 h (no accumulation, Fig. 2b) agrees very well with the CTM predictions, with RMSEs and NMBs within 4 ppb and ± 1%, respectively, and R^2 values close to 1.

Due to the chaotic nature of the atmospheric system (Brasseur and Jacob, 2017), a small error in the initial condition can be amplified in the subsequent prediction steps, which creates challenges for any time-series prediction for the atmosphere system. To further examine the model performance in predicting O_3 through a long-time period rather than at the sixth hour as set in the training process, we use the prior-predicted O_3 and NO_2 as the initial conditions to feed into the prediction for the following steps. As the DeepCTM integration proceeds over multiple time steps, the small errors for individual steps can accumulate slightly (Fig. 2a). However, the implementation of LSTM can well control the error accumulation within certain range. The RMSEs increase to 5.4 ppb at the 12th hour (through 1 time accumulation, Fig. 2c), and 5–6 ppb at the 24th hour (through 3 time accumulation, Fig. 2d). However, the RMSEs are kept around 5–6 ppb in the following predictions for days 2–7 (through 7 to 27 time accumulation) (Fig. 2e-g). The NMBs also continually increase with the time integration but remain within 10% (the largest NMB values occur at low baseline O_3 levels) during the 7 day period (Fig. 2a), suggesting that implementation of the recurrent network structure like LSTM can well reduce the rate of error accumulation; though error accumulation remains as the biggest challenge for long-time prediction with any time-accumulation based method like DeepCTM.

We also examine the trained DeepCTM in predicting the simulation of other cases (Case 5–8) with the variation of emissions and meteorological conditions (Fig. S6–7). In general, the DeepCTM can also well capture the magnitudes and range of hourly O_3 concentrations across all cases, with acceptable NMBs (mostly within ±20%) (see in Fig. S6), even though the prediction is initialized only at the first 6 h of each month (i.e., multiple steps with accumulation). Relatively worse performance with larger NMB is shown in Case 2, 4, 7 and 8 simulated with higher NO_x emissions which lead to extremely low O_3 values in winter (strong VOC-limited) as the small denominator for NMB calculation. Surely the performance of DeepCTM can be further improved by using a wider range of emission data for training to better represent these conditions. The DeepCTM can also well capture the spatial distribution of O_3 concentration even through a whole month accumulation, with small RMSE (2–3 ppb) and high R^2 (>0.9) (Fig. S7). That implies the DeepCTM can mimic the CMAQ simulations just with its inputs (initial condition at the first 6 h and meteorological data) continually for the whole months.

3.2. Identification of the factors that dominate O_3 diurnal variation

Lack of interpretability is one shortcoming for most machine learning-based models; however, the ability of the DeepCTM in predicting O_3 can be explored through sensitivity analysis by modulating the input features. Specifically, the importance of each feature for the DeepCTM prediction can be quantified by the change of the predicted O_3 associated with a change in the feature. To better understand how the DeepCTM can capture the change of O_3 from Case 1 to Case 4 (Fig. S8), we quantify the contribution from each input feature to the change of O_3 prediction from Case 1 to Case 4. A series of hypothetical cases were conducted by using data for one feature from Case 4 with the remaining

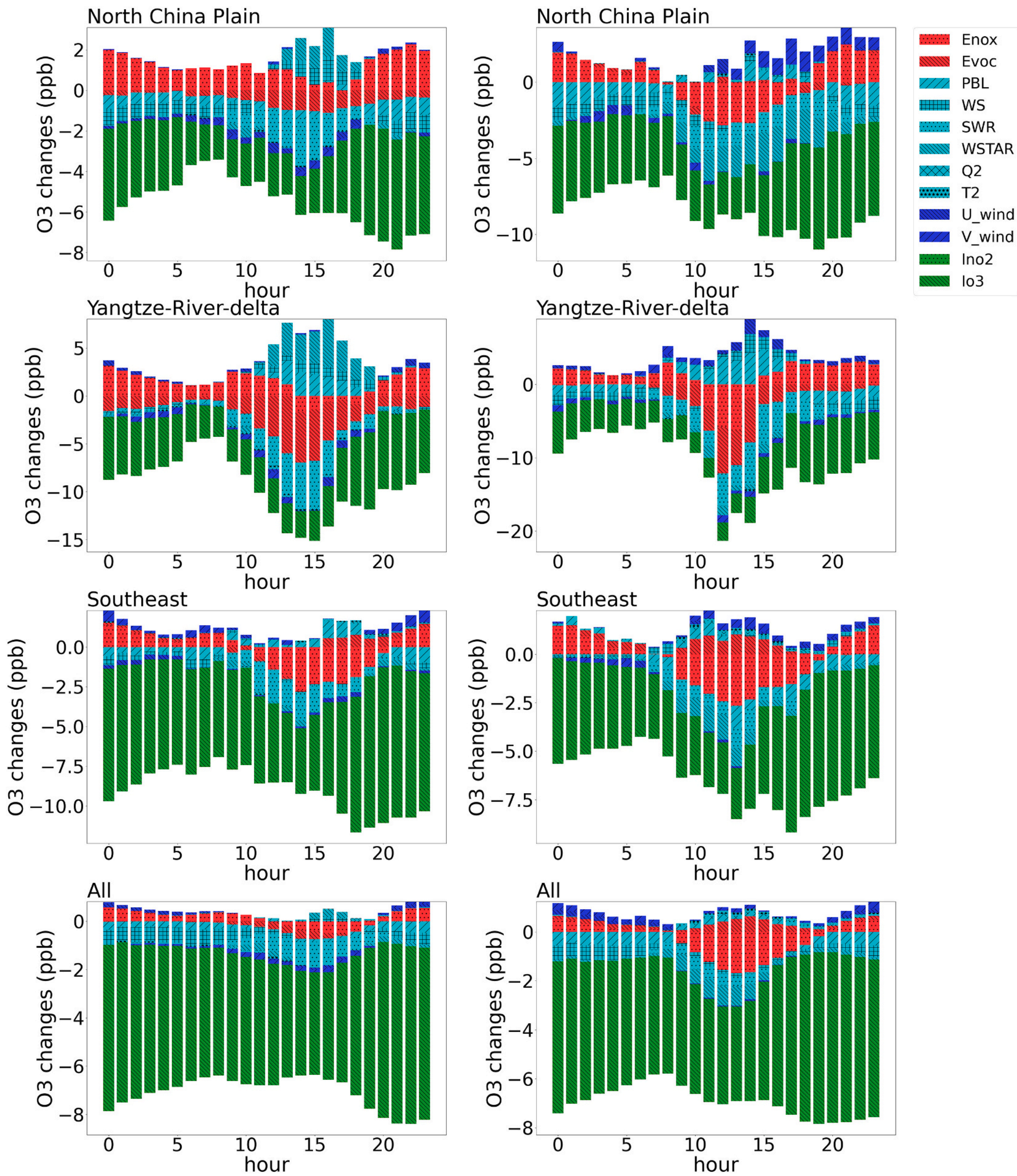

Fig. 3. The O_3 sensitivities to the variation of individual factors (emission, initial condition, flux transport, and other meteorological factors are marked as red, green, blue, and cyan respectively; all factors are quantified through a 20% variation, except for T2 through a 2 K reduction). (For interpretation of the references to colour in this figure legend, the reader is referred to the web version of this article.)

features kept the same as in Case 1, and repeating the process for all features. Therefore the difference between the predicted O_3 in the hypothetical case and Case 1 can be regarded as the individual contribution from the feature modulated in the hypothetical case. The results show that the decreased O_3 in southern China is mainly driven by the change of short-wave radiation (ΔSWR) and flux transport (ΔUV-wind), while the increased O_3 in northern (in January) and western China (in July) is mostly driven by the PBL height (ΔPBL). Note that we modulate each feature one-by-one and thus the sum of the individual contributions is not equal to the total changes due to nonlinearity in the underlying system.

To further examine the influence of individual factors on the diurnal variation of O_3, we conducted a sensitivity analysis by modulating each feature one-by-one in predicting the O_3 response with DeepCTM across two typical days (Fig. 3). The features of emission (Enox, Evoc), initial conditions (Ino2, Io3), flux transport (U_wind, V_wind) and meteorological factors (i.e., PBL, WS, SWR, WSTAR, and Q2) are set with a 20% reduction, except for T2 which are set with a reduction of 2 K. The small perturbations are within the range of variation in the training data to ensure its accuracy from the DeepCTM prediction.

The 24-h DeepCTM predictions (initialized for each hour with no accumulation) suggest that the initialized O_3 concentration is the dominant factor contributing to O_3 across a day (Fig. 3). The influence of the initial condition of O_3 decays slowly from morning till the noon and then increases again overnight, indicating the photochemical formation of O_3 during daytime reduces the importance of the initial conditions. Such large influence of initial condition to the diurnal variation of O_3 is mainly because of the single-step running without accumulation. The impacts of initial condition will be slowly reduced along with the accumulation, and the DeepCTM can also well capture such decay of the initial impacts (Fig. S9).

The flux transport factor (U_wind and V_wind) influences O_3 concentration changes through regional transport. In the three polluted regions, the O_3 flux transport acts as a sink during daytime. This

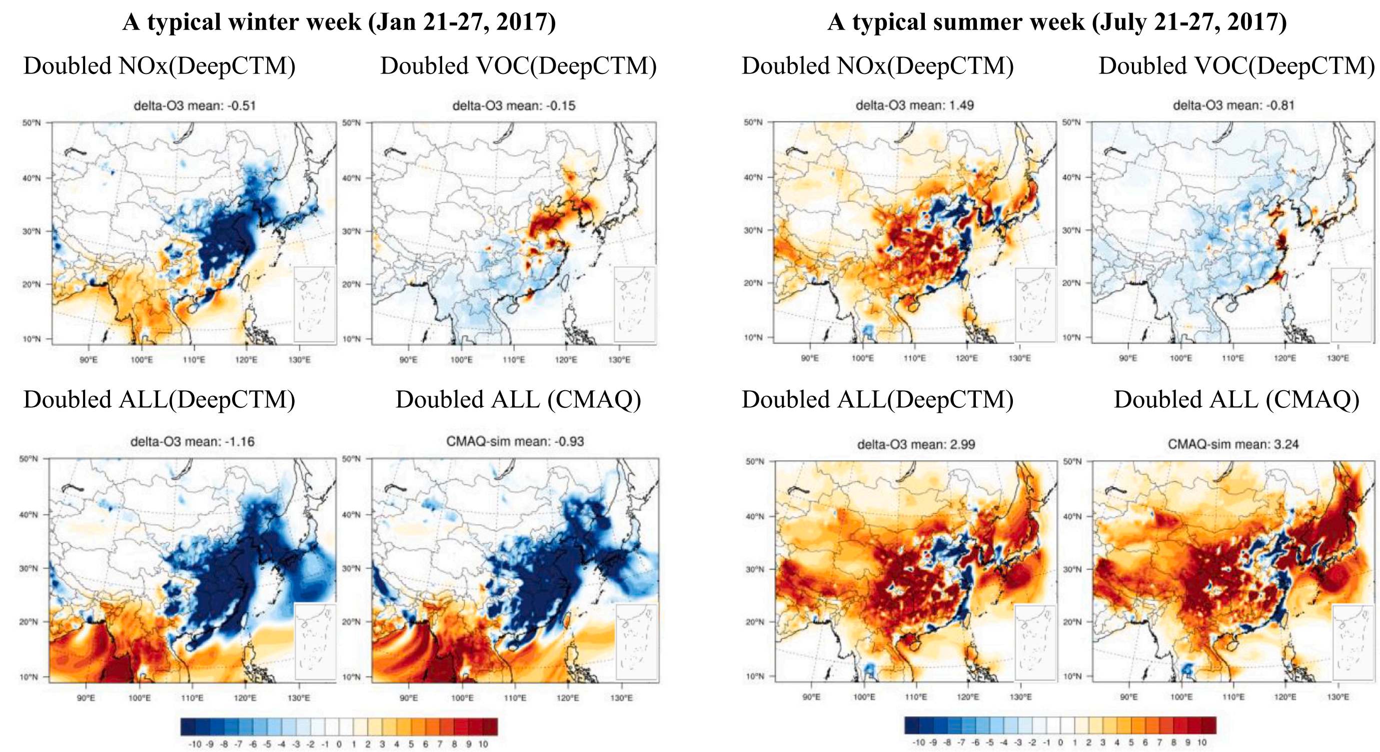

Fig. 4. Prediction of O_3 response to doubled emission of NO_x and VOC (unit: ppbV, initializing at the first 6 h and accumulating through the whole week).

behavior is due to the transport of locally formed O_3 to downwind areas that reduces O_3 in the source region. Such phenomena are most pronounced in summer. The flux transport can be also a source in polluted regions at night and in winter. That might be associated with the movement of NO_x out of the polluted region which will reduce the O_3 loss at night due to NO titration and oxidant limitations and thereby enhance the O_3 concentration. Such detailed chemical behaviors are well captured by the DeepCTM.

The meteorology factors exert considerable influence on O_3 mostly during daytime when O_3 is formed through photochemical reactions. The 20% reduction in surface short-wave radiation mitigates O_3 formation during daytime. Similarly, the 2-K reduction in 2-m temperature slightly reduces O_3 in most regions in winter due to its influence on chemical reaction rates. However, the opposite impact of 2-m temperature on O_3 occurs in the southern regions in summer likely because lower temperatures are associated with higher biogenic VOC emissions which can consume the O_3 sharply under NOx-limited conditions. The 20% reduction in PBL height and wind speed slightly increase the daytime O_3 concentrations, probably due to the enhancement of precursor concentrations that promote O_3 formation, while they reduce O_3 concentrations at night due to the transition of O_3 chemistry to VOC-limited conditions. The reduction of convective velocity scale (WSTAR) also exhibits strong impacts on daytime O_3 by reducing O_3 in summer and increasing O_3 in winter. Such behavior might be associated with the vertical transport of O_3 and precursors. The reduced convective velocity scale leads to reduced O_3 due to the weaker vertical mixing that transports upper-level O_3 downward to surface in summer. However, the reduced convective velocity scale increases O_3 in winter, probably due to the reduced NO_x concentrations under VOC-limited regime. A similar finding is indicated by the seasonality of meteorological influences on O_3 with initialized at first 6 h in each month (i.e., multiple steps with accumulation) (detailed in Text S1 and Fig. S10).

The precursor emissions can either be a source or sink for O_3 across a day. Surface NO_x emissions contribute to daytime O_3 formation but tend to reduce O_3 at night when NO_x consumes O_3 through direct reaction. VOC emission reductions are always beneficial for reducing O_3 in North China Plain and Yangtze-River-Delta, while they slightly enhance O_3 in Southeast and all China in summer, probably due to the active VOC species associated with biogenic sources consuming O_3 under low NO_x conditions. Note that here we conducted the sensitivity analysis with emissions of each species individually adjusted. Simultaneous control of the precursors leads to a more complex O_3 response, which is discussed next.

3.3. Prediction of the nonlinear O_3 response to precursor emission changes

Using the DeepCTM, the isopleth of O_3 concentration for variations in precursor emissions can easily be predicted as done with response surface models (RSMs) (Xing et al., 2011b, 2017a). The O_3 responses to the change of NO_x and VOC emissions by a range of ratios from 0 to 2 (for zero-out to double emissions) were predicted by DeepCTM for two typical hours (6 am and 12 pm) in two typical days (Fig. S11) with single-step (no accumulation). In general, the responses of O_3 to total NO_x and VOC emissions are quite similar as we found in previous RSM studies (Xing et al., 2011b, 2017a, 2020c). The O_3 chemistry is mostly in a NO_x-limited regime in summer and at noon and in southern regions like Southeast, but in a VOC-limited regime in winter and in northern regions like North China Plain. The results about O_3 chemistry regime are consistent with previous studies. For example, Wang et al. (2019a, 2019b) and Lyu et al. (2019) found VOC-limited regime in eastern China and North China Plain. While, Li et al. (2013) reported NOx-limited regime in Pearl River Delta region at noon time.

Such strong spatial and seasonal variation of O_3 chemistry is also suggested from the O_3 responses to the doubling of NO_x and VOC emissions (from Case 1 to Case 2) (see Fig. 4). In general, the DeepCTM has successfully captured the decreased O_3 in winter and increased O_3 in summer in most of China. The model also well captured the increased O_3 in the south (with limited NO_x emissions and strongly NO_x-limited conditions) in winter as well as the decreased O_3 in polluted regions like Northern China Plain (with abundant NO_x emissions and at strongly VOC-limited conditions). Such changes are mostly driven by the doubling of NO_x emissions. One thing should be noted that the double

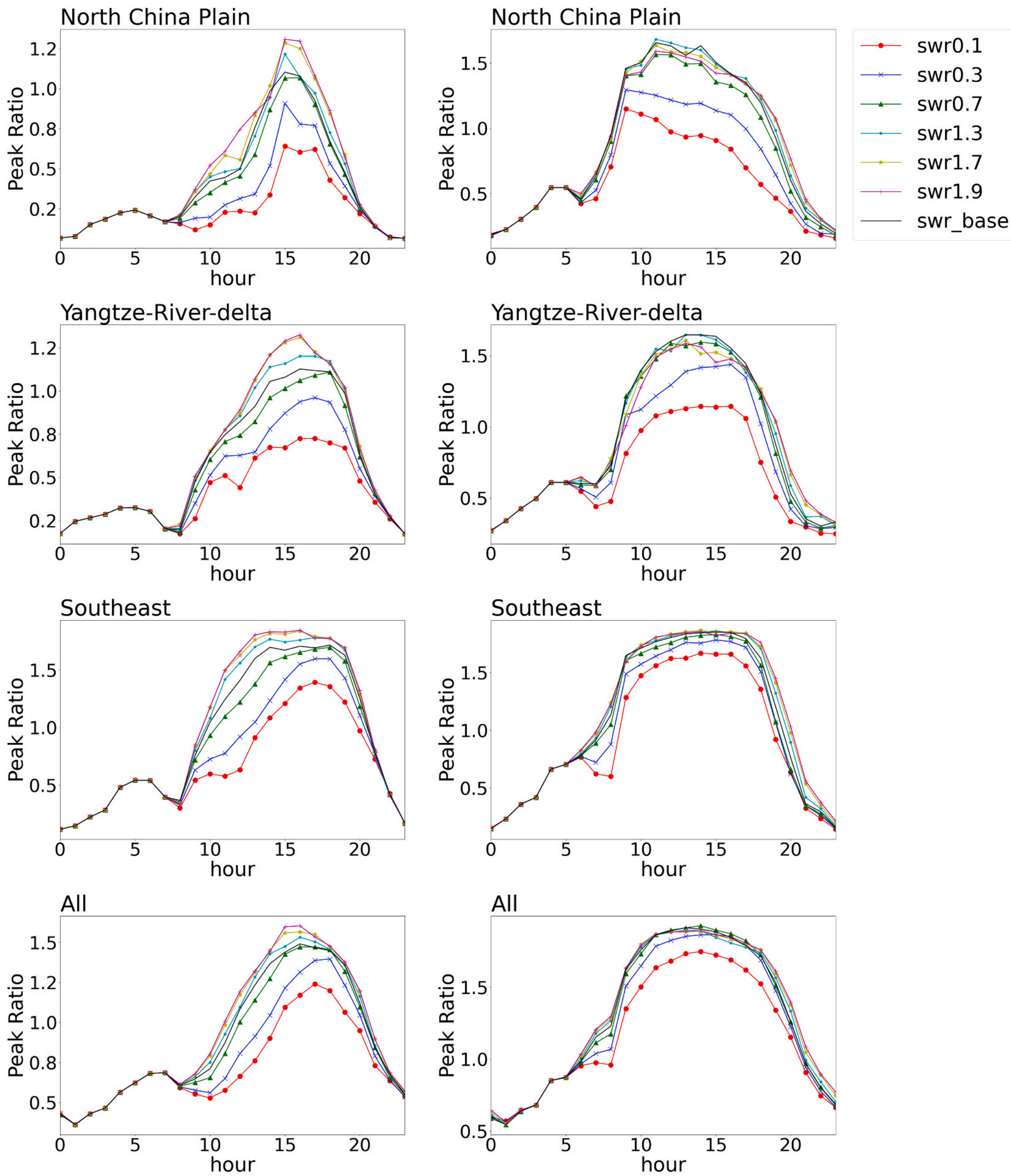

Fig. 5. The O_3 chemistry (indicated by the Peak Ratio) response to the variation of short-wave radiation across a day.

VOC might slightly decrease O_3 mostly in the rural areas where with high biogenic VOCs which can consume the O_3 sharply under NOx-limited conditions. However, uncertainties are still existed due to the DeepCTM limitation in dealing with the VOC speciation which need be further implemented into the model design.

In addition to reduced requirements for CTM simulations for model development, another advantage of the DeepCTM over the RSM is the ability of the DeepCTM to explore the influence of meteorology variations on O_3 chemistry. We conducted such investigation using the Peak Ratio (Xing et al., 2019a), which is an indicator of the chemical regime for the O_3 response to precursor changes. The Peak Ratio is the NO_x emission change ratio (range of 0 to 2 for zero-out to double emissions) corresponding to the maximum O_3 concentration under conditions of baseline VOC emissions. O_3 chemistry is in the VOC-limited regime when Peak Ratio < 1 and in the NOx-limited regime when Peak Ratio > 1. The influence of meteorology variations on O_3 chemistry is examined by comparing the Peak Ratio response to the variation of each meteorological factor.

Fig. 5 presents the diurnal Peak Ratio across a day under seven levels of short-wave radiation, including the baseline (swr_base), 90% reduced (swr0.1), 70% reduced (swr0.3), 30% reduced (swr0.7), 30% increased (swr1.3), 70% increased (swr1.7), and 90% increased (swr1.9) radiation. For baseline conditions, the Peak Ratio exhibits strong diurnal variation with the highest value at noon and lowest value at night. This behavior indicates that O_3 chemistry is much more likely to be in the NO_x-limited regime at noon and in the VOC-limited at night. The summertime Peak Ratio is also always higher than that in winter implying the stronger NO_x-limited regime in warmer seasons when oxidants are abundant.

The variation of short-wave radiation can significantly modulate the O_3 chemistry across the day in both seasons. In general, reductions in short-wave radiation will lower the Peak Ratio leading the O_3 chemistry toward the VOC-limited regime and increases in radiation will enlarge the Peak Ratio leading the O_3 chemistry toward the NO_x-limited regime. This behavior is because stronger short-wave radiation favors the photolysis of NO_2 to form O_3, whereas the consumption of OH by NO_2 (which terminates radical reactions and thus reduces O_3 formation) is favored under conditions of weaker short-wave radiation. The change in

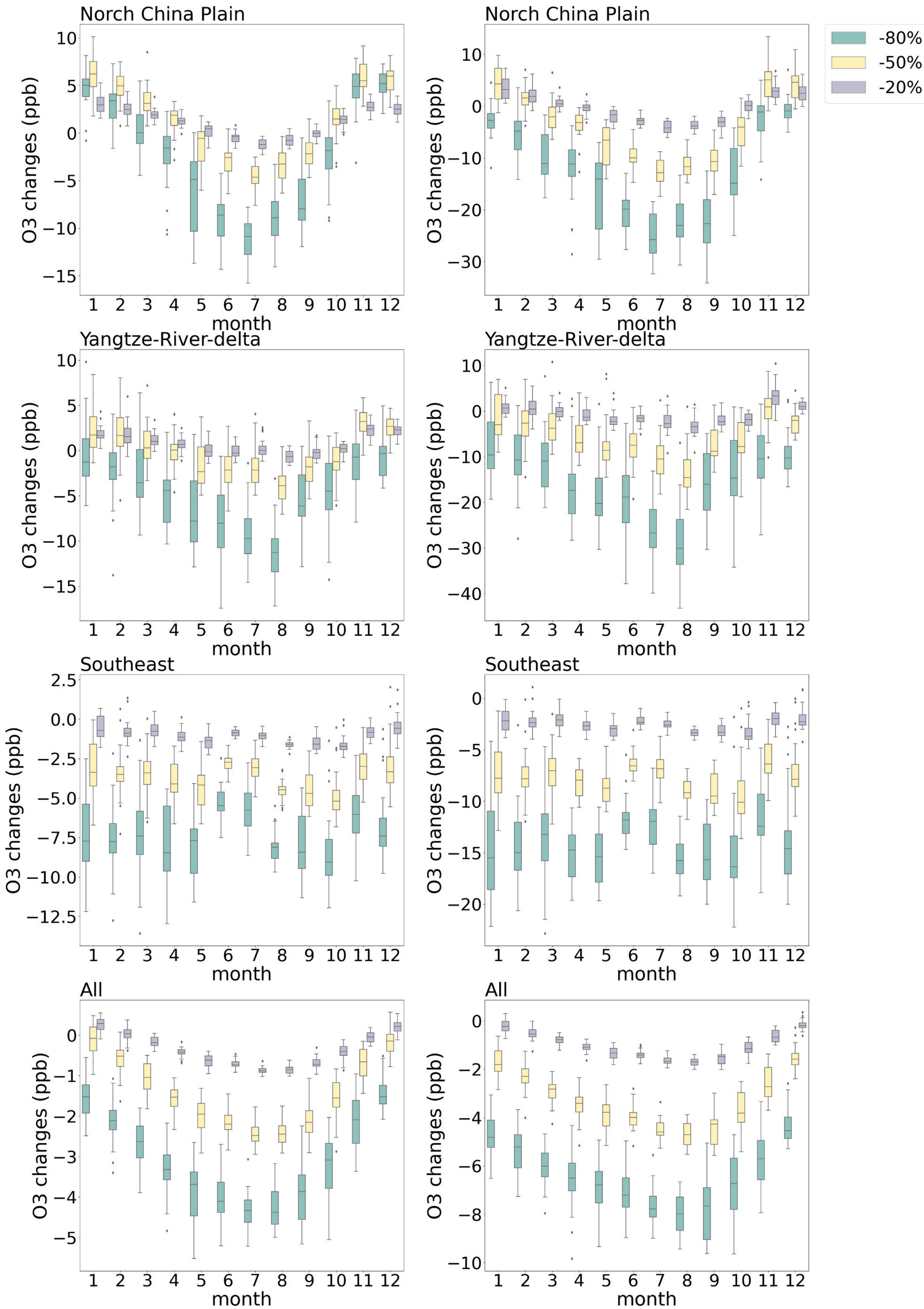

Fig. 6. The O_3 changes due to NO_x emission controls under different meteorological conditions across a year.

O_3 chemistry associated with short-wave radiation is more pronounced in the North China Plain in winter, indicating that north regions and colder seasons (with less baseline radiation) are more sensitive to short-wave radiation than other regions/seasons. Meanwhile, meteorological factors in addition to short-wave radiation also influenced the O_3 chemistry (detailed in Text S2, Fig. S12–15).

3.4. Seasonality of meteorological influences on O_3 response to NO_x emission reductions

To examine the meteorological influence on the O_3 response to NO_x emission reductions, we compared the daily O_3 response to NO_x emission reductions in different months by considering 20%, 50%, and 80% NO_x control (Fig. 6). We conducted this analysis by applying the DeepCTM with initialized at first 6 h on each day (multiple step with accumulation).

Results suggest strong seasonality in the O_3 response to emission changes. In general, NO_x control is beneficial for reducing O_3 in summer, but disbeneficial or ineffective for reducing O_3 in winter. One thing should be noted that the benefits of NO_x control highly depends on its reduction ratio, as the 20% control has very limited benefits on O_3 reduction while the benefits of NO_x controls increase substantially when contorl ratio reachs 80%. Such findings are consistent with our previous study (Xing et al., 2018), demonstrating the strong nonlinearity of O_3 responses to NO_x emission reductions due to the meteorological variations. Even in a single month, there are a wide range of O_3 responses to NO_x emission changes, with variations of 5–10 ppb and both negative and positive responses. These results demonstrate that meteorological variations can have a large influence on the control effectiveness even at a small temporal scale (e.g., day-to-day variations), which should be considered in designing effective control strategies.

4. Conclusion

The deep learning-based air quality simulator (i.e., DeepCTM) proposed in this study exhibits its ability in reproducing the temporal and spatial patterns of O_3 concentrations, as well as its inner correlations with precursor emissions and meteorological factors. One potential application of the DeepCTM is 7-day forecasting as the well-trained DeepCTM can accurately and efficiently predict the O_3 variations with emissions and meteorology over 7 days of continual forecasting with limited accumulated errors. Since all the inputs of DeepCTM are ready with no additional CTM simulations (initial condition can be derived from current status fused with observations), the application of DeepCTM can significantly improve the real-time prediction of air quality and inform policymakers to mitigate air pollution, by designing effective control strategies from efficient prediction of multiple emission control scenarios (Xing et al., 2017b, 2019b).

The DeepCTM also successfully identified the dominate factors that contribute to the O_3 diurnal variation and captured the nonlinearity of O_3 response to emissions under different meteorological conditions, exhibiting the advantage of high efficiency in identifying the dominant factor to photochemical formation over existing CTM-based methods. Besides, the emission-meteorology-concentration linkages implied by the DeepCTM are consistent with known mechanisms of atmospheric chemistry, indicating that the DeepCTM is also scientifically reasonable. These results suggest that the neural-network-based predictor can represent the basic physical and chemical processes of the atmosphere from the raw CTM-simulated data, which further implies an important fact that for systems that can be represented deterministically (e.g., atmospheric air pollution), we can generally mimic the full pathway using information from the initial and crucial features alone.

This study also reveals that the implementation of time-series neural network structure will address the error accumulation problem which is one challenge for long-time prediction. The initial errors grow slightly during the time integration but then become stable even up to a week of accumulation. More accurate representation of the CTM structure would help to further improve the accuracy of DeepCTM. For example, in this study we simplified the vertical structure of the atmosphere by only selecting the surface features to represent the atmospheric system. Apparently, such simplification might lead to systemic errors in DeepCTM predictions, and inclusion of additional features in the neural network could be necessary to address these issues. This is a challenging task since the training with inclusion of the vertical parameters would require >10 times the computational resources, which might need further improvement of model design with implementation of dimensionality reduction techniques, such as auto-decoder or 3-D CNN to exact the information from the vertical structure of the atmosphere. Also, since training is done using three CTM simulations, errors can occur in predicting conditions not included in the training set, like the extremely low VOC emissions in summer. Such biases can be reduced by incorporating CTM simulations for multiple emission control scenarios into the training dataset. In the current DeepCTM design, we did not include the concentration of individual VOC species due to the complex chemical mechanisms for VOCs that vary among CTMs. Incorporating additional species would increase the computational demand for training the DeepCTM and would significantly enlarge the influence of initial conditions and thus the error accumulation. The above issues are recommended for future studies. Nevertheless, the DeepCTM proposed in this study demonstrates its large advantage and potential for addressing the complicated atmospheric system, which can be continually improved with further efforts in both environmental scientific research and computational technologies.

Code/data availability

The original data and code used in this study are available upon request from the corresponding authors.

Competing interests

The authors declare that they have no conflict of interest.

Disclaimer

The views expressed in this manuscript are those of the authors alone and do not necessarily reflect the views and policies of the U.S. Environmental Protection Agency.

Declaration of Competing Interest

None.

Acknowledgements

This work was supported in part by Shanghai Science and Technology Commission Scientific Research Project (19DZ1205006), National Natural Science Foundation of China (41907190), National Key R & D program of China (2018YFC0213805), and MSRA collaborative research project. This work was completed on the “Explorer 100” cluster system of Tsinghua National Laboratory for Information Science and Technology.

Appendix B. Supplementary data

Seasonality of meteorological influences on O_3; Text S2: The influence of other meteorological factors on O_3 chemistry; Fig. S1-S15. Supplementary data to this article can be found online at https://doi.org/10.1016/j.atmosres.2021.105919.

References

Appel, K.W., et al., 2013. Evaluation of dust and trace metal estimates from the Community Multiscale Air Quality (CMAQ) model version 5.0. Geosci. Model Dev. 6 (4), 883–899.

Appel, K.W., et al., 2018. Overview and Evaluation of the Community Multiscale Air Quality (CMAQ) Modeling System Version 5.2. Air Pollution Modeling and its Application Xxv, pp. 69–73. https://doi.org/10.1007/978-3-319-57645-9_11.

Brasseur, G.P., Jacob, D.J., 2017. Modeling of Atmospheric Chemistry. Cambridge University Press.

Cabaneros, S.M.S., Calautit, J.K., Hughes, B.R., 2019. A review of artificial neural network models for ambient air pollution prediction. Environ. Model. Softw. 119, 285–304.

Cohan, D.S., Hakami, A., Hu, Y., Russell, A.G., 2005. Nonlinear response of ozone to emissions: source apportionment and sensitivity analysis. Environ. Sci. Technol. 39, 6739–6748.

Csáji, B.C., 2001. Approximation with artificial neural networks, 24(48). Faculty of Sciences, Etvs Lornd University, Hungary, p. 7.

Ding, D., Xing, J., Wang, S., Chang, X., Hao, J., 2019a. Impacts of emissions and meteorological changes on China's ozone pollution in the warm seasons of 2013 and 2017. Front. Environ. Sci. Eng. 13 (5), 1–9.

Ding, D., Xing, J., Wang, S., Liu, K., Hao, J., 2019b. Estimated contributions of emissions controls, meteorological factors, population growth, and changes in baseline mortality to reductions in ambient PM2.5 and PM2.5 -related mortality in China, 2013–2017. Environ. Health Perspect. 127 (6), 67009.

Dunker, A.M., Yarwood, G., Ortmann, J.P., Wilson, G.M., 2002. Comparison of source apportionment and source sensitivity of ozone in a three-dimensional air quality model. Environ. Sci. Technol. 36, 2953–2964.

Gilliland, A.B., Hogrefe, C., Pinder, R.W., Godowitch, J.M., Foley, K.L., Rao, S.T., 2008. Dynamic evaluation of regional air quality models: Assessing changes in O3 stemming from changes in emissions and meteorology. Atmos. Environ. 42 (20), 5110–5123.

Gipson, G.L., Freas, W.P., Kelly, R.F., Meyer, E.L., 1981. Guideline for use of city-specific EKMA in preparing ozone SIPs. In: EPA-450/4–80-027. USA, US Environmental Protection Agency, Research Triangle Park, North Carolina.

Goyal, A., Bengio, Y., 2020. Inductive biases for deep learning of higher-level cognition. In: arXiv preprint. arXiv:2011.15091.

Grulke, N.E., Heath, R.L., 2020. Ozone effects on plants in natural ecosystems. Plant Biol. 22, 12–37.

Guenther, A.B., Jiang, X., Heald, C.L., Sakulyanontvittaya, T., Duhl, T., Emmons, L.K., Wang, X., 2012. The Model of Emissions of gases and Aerosols from Nature version 2.1 (MEGAN2. 1): an extended and updated framework for modeling biogenic emissions. Geosci. Model Dev. 5 (6), 1471–1492.

Hong, C., et al., 2019. Impacts of climate change on future air quality and human health in China. Proc. Natl. Acad. Sci. 116 (35), 17193–17200.

Hsieh, J.T., et al., 2019. Learning Neural PDE Solvers with Convergence Guarantees (International Conference on Learning Representations).

Hu, C., Kang, P., Jaffe, D.A., et al., 2021. Understanding the impact of meteorology on ozone in 334 cities of China. Atmos. Environ. 248, 118221.

Huang, L., Liu, S., Yang, Z., Xing, J., Zhang, J., Bian, J., Li, S., Sahu, S.K., Wang, S., Liu, T.-Y., 2021. Exploring deep learning for air pollutant emission estimation. Geosci. Model Dev. 14, 4641–4654. https://doi.org/10.5194/gmd-14-4641-2021.

Kelp, M.M., Jacob, D.J., Kutz, J.N., Marshall, J.D., Tessum, C.W., 2020. Toward stable, general machine-learned models of the atmospheric chemical system. J. Geophys. Res.-Atmos. 125 (23) e2020JD032759.

Kwok, R.H.F., Baker, K.R., Napelenok, S.L., Tonnesen, G.S., 2015. Photochemical grid model implementation and application of VOC, NOx, and O3 source apportionment. Geosci. Model Dev. 8, 99–114.

Li, Y., Lau, A.K.H., Fung, J.C.H., Zheng, J., Liu, S., 2013. Importance of NOx control for peak ozone reduction in the Pearl River Delta region. J. Geophys. Res.-Atmos. 118 (16), 9428–9443.

Liu, et al., 2021. Health benefits of emission reduction under 1.5°C pathways far outweigh climate-related variations in China. Environ. Sci. Technol. https://doi.org/10.1021/acs.est.1c01583.

Lu, X., Zhang, S., Xing, J., Wang, Y., Chen, W., Ding, D., , et al.Hao, J., 2020. Progress of air pollution control in China and its challenges and opportunities in the ecological civilization era. Engineering 6 (12), 1423–1431.

Lyu, X., et al., 2019. Causes of a continuous summertime O3 pollution event in Jinan, a central city in the North China Plain. Atmos. Chem. Phys. 19, 3025–3042.

Ma, M., Gao, Y., Wang, Y., Zhang, S., Leung, L.R., Liu, C., et al., 2019. Substantial ozone enhancement over the North China Plain from increased biogenic emissions due to heat waves and land cover in summer 2017. Atmos. Chem. Phys. 19 (19), 12195–12207.

Murray, C.J., Aravkin, A.Y., Zheng, P., Abbafati, C., Abbas, K.M., Abbasi-Kangevari, M., Borzouei, S., 2020. Global burden of 87 risk factors in 204 countries and territories, 1990–2019: a systematic analysis for the Global Burden of Disease Study 2019. The Lancet 396 (10258), 1223–1249.

Orhan, E., Pitkow, X., 2018. Skip connections eliminate singularities. In: International Conference on Learning Representations.

Santurkar, S., et al., 2018. How does batch normalization help optimization?. In: Proceedings of the 32nd International Conference on Neural Information Processing Systems, pp. 2488–2498.

Sarwar, G., Luecken, D., Yarwood, G., Whitten, G.Z., Carter, W.P.L., 2008. Impact of an updated carbon bond mechanism on predictions from the CMAQ modeling system: preliminary assessment. J. Appl. Meteorol. Climatol. 47 (1), 3–14.

Seinfeld, J.H., Pandis, S.N., 2012. Atmospheric Chemistry and Physics: From Air Pollution to Climate Change. John Wiley & Sons.

Skamarock, W.C., Klemp, J.B., Dudhia, J., Gill, D.O., Barker, D.M., Duda, M.G., Huang, X.-Y., Wang, W., Powers, J.G., 2008. A Description of the Advanced Research WRF Version 3. NCAR Tech. Note NCAR/TN-475+STR, 113 pp.

Stowell, J.D., Kim, Y.M., Gao, Y., Fu, J.S., Chang, H.H., Liu, Y., 2017. The impact of climate change and emissions control on future ozone levels: Implications for human health. Environ. Int. 108, 41–50.

Turnock, S.T., Wild, O., Dentener, F.J., Davila, Y., Emmons, L.K., Flemming, J., Folberth, G.A., Henze, D.K., Jonson, J.E., Keating, T.J., Kengo, S., Lin, M., Lund, M., Tilmes, S., O'Connor, F.M., 2018. The impact of future emission policies on tropospheric ozone using a parameterised approach. Atmos. Chem. Phys. 18, 8953–8978. https://doi.org/10.5194/acp-18-8953-2018.

Wang, P., Guo, H., Hu, J., Kota, S.H., Ying, Q., Zhang, H., 2019a. Responses of PM2. 5 and O3 concentrations to changes of meteorology and emissions in China. Sci. Total Environ. 662, 297–306.

Wang, N., Lyu, X., Deng, X., Huang, X., Jiang, F., Ding, A., 2019b. Aggravating O3 pollution due to NOx emission control in eastern China. Sci. Total Environ. 677, 732–744.

Wang, Y., Wild, O., Chen, X., Wu, Q., Gao, M., Chen, H., et al., 2020. Health impacts of long-term ozone exposure in China over 2013-2017. Environ. Int. 144, 106030.

Wild, O., Fiore, A.M., Shindell, D.T., Doherty, R.M., Collins, W.J., Dentener, F.J., Schultz, M.G., Gong, S., MacKenzie, I.A., Zeng, G., Hess, P., Duncan, B.N., Bergmann, D.J., Szopa, S., Jonson, J.E., Keating, T.J., Zuber, A., 2012. Modelling future changes in surface ozone: a parameterized approach. Atmos. Chem. Phys. 12, 2037–2054. https://doi.org/10.5194/acp-12-2037-2012.

Womack, C.C., et al., 2019. An odd oxygen framework for wintertime ammonium nitrate aerosol pollution in urban areas: NOx and VOC control as mitigation strategies. Geophys. Res. Lett. 46 (9), 4971–4979.

Xing, J., et al., 2011a. Modeling study on the air quality impacts from emission reductions and atypical meteorological conditions during the 2008 Beijing Olympics. Atmos. Environ. 45 (10), 1786–1798.

Xing, J., Wang, S.X., Jang, C., Zhu, Y., Hao, J.M., 2011b. Nonlinear response of ozone to precursor emission changes in China: a modeling study using response surface methodology. Atmos. Chem. Phys. 11, 5027–5044.

Xing, J., Wang, S., Zhao, B., Wu, W., Ding, D., Jang, C., Zhu, Y., Chang, X., Wang, J., Zhang, F., Hao, J., 2017a. Quantifying Nonlinear Multiregional Contributions to ozone and Fine Particles using an Updated Response Surface Modeling Technique. Environ. Sci. Technol. 51 (20), 11788–11798.

Xing, J., Wang, S., Jang, C., Zhu, Y., Zhao, B., Ding, D., Wang, J., Zhao, L., Xie, H., Hao, J., 2017b. ABaCAS: An Overview of the Air Pollution Control Cost-Benefit and Attainment Assessment System and its Application in China. The Magazine for Environmental Managers - Air & Waste Management Association. April.

Xing, J., Ding, D., Wang, S., Zhao, B., Jang, C., Wu, W., Zhang, F., Zhu, Y., Hao, J., 2018. Quantification of the enhanced effectiveness of NOx control from simultaneous reductions of VOC and NH3 for reducing air pollution in the Beijing–Tianjin–Hebei region, China. Atmos. Chem. Phys. 18, 7799–7814.

Xing, J., Ding, D., Wang, S., Dong, Z., Kelly, J.T., Jang, C., Zhu, Y., Hao, J., 2019a. Development and application of observable response indicators for design of an effective ozone and fine particle pollution control strategy in China. Atmos. Chem. Phys. 19 (21), 13627–13646.

Xing, J., Wang, S., Zhu, Y., Ding, D., Long, S., Tian, H., Jang, C., Hao, J., 2019b. Development and Application of the Scientific Decision support Platform for Air Pollution Prevention and Control. Res. Environ. Sci. 10.

Xing, J., et al., 2020a. Data assimilation of ambient concentrations of multiple air pollutants using an emission-concentration response modeling framework. Atmosphere 11 (12), 1289.

Xing, J., et al., 2020b. Quantifying the emission changes and associated air quality impacts during the COVID-19 pandemic on the North China Plain: a response modeling study. Atmos. Chem. Phys. 20 (22), 14347–14359.

Xing, J., et al., 2020c. Deep learning for prediction of the air quality response to emission changes. Environ. Sci. Technol. 54 (14), 8589–8600.

Xing, J., et al., 2020d. The quest for improved air quality may push China to continue its CO2 reduction beyond the Paris Commitment. Proc. Natl. Acad. Sci. 117 (47), 29535–29542.

Yang, X., Wu, K., Lu, Y., Wang, S., Qiao, Y., Zhang, X., et al., 2021. Origin of regional springtime ozone episodes in the Sichuan Basin, China: role of synoptic forcing and regional transport. Environ. Pollut. 116845.

Zheng, H., et al., 2019. Transition in source contributions of PM 2.5 exposure and associated premature mortality in China during 2005–2015. Environ. Int. 475, 132.